Available online at www.sciencedirect.com

ScienceDirect

Ceramics International 40 (2014) 1279–1288

CERAMICS INTERNATIONAL

www.elsevier.com/locate/ceramint

Structural, optical and magnetic properties of $Zn_{0.97-x}Al_xCr_{0.03}S$ nanoparticles

D. Amaranatha Reddy[a,*], Chunli Liu[a], R.P. Vijayalakshmi[b], B.K. Reddy[b]

[a]Department of Physics, Hankuk University of Foreign Studies, Yongin 449-791, Republic of Korea
[b]Department of Physics, Sri Venkateswara University, Tirupati 517502, India

Received 19 June 2013; accepted 1 July 2013
Available online 13 July 2013

Abstract

$Zn_{0.97-x}Al_xCr_{0.03}S$ ($x=0.00$, 0.02, 0.04, 0.06, 0.08, 0.10 and 0.12) nanoparticles were synthesized by the chemical co-precipitation method using Ethylene Di-amine Tetra Acetic acid (EDTA) as capping agent. The effect of Al co-dopant on the structural, optical and magnetic properties is discussed on the basis of EDS, SEM, XRD, TEM, SAED, DRS, FTIR, PL, EPR and VSM results. EDS studies indicated the presence of Zn, S, Cr and Al elements in the samples with near stoichiometry. XRD, TEM and SAED studies revealed that samples of all concentrations exhibited cubic structure. The absorption edge in DRS spectra shifted towards higher wavelength with increasing Al concentration indicating a decrease of band gap from 4.05 to 3.85 eV. Enhanced photoluminescence was observed with increasing Al concentration up to 4 at% and beyond this photoluminescence quenching was observed. FTIR spectral studies indicated that EDTA simply co-exists on the surface of the nanoparticles and acts as the capping agent preventing agglomeration of the nanoparticles. EPR spectral studies indicated that the EPR signal intensity, linewidth and number of spins increased with Al concentration. VSM studies revealed that Al co-doping suppressed the room temperature ferromagnetism in ZnS:Cr nanoparticles.

Keywords: ZnS:(Cr, Al); Chemical method; XRD; DRS; Absence of room temperature ferromagnetism

1. Introduction

In recent years, scientists have made rapid and significant advances in the field of materials research, especially in semiconductor physics. One of the most important fields of current interest in materials science is discovery and understanding of Room Temperature Ferromagnetic (RTFM) semiconductors with Curie point (T_c) above room temperature. It is a difficult task to find Diluted Magnetic Semiconductors (DMS) with room temperature ferromagnetism. DMS are a class of magnetic semiconductors that are obtained by adding a fraction of transition or rare earth metal ions such as Mn, Fe, Co, Cr, Ni, Cu, Sm, Er, Dy, and Gd to II–VI, IV–VI and III–V compounds [1]. These DMS can exploit both the charge and spin of carriers, with the concept of the synergetic and multifunctional use of spin and charge dynamics of electrons, aiming to go beyond the traditional dichotomy of semiconductor electronics and magnetic storage technology. Their possible applications in the next generation spintronic devices like non-volatile storage, spin light-emitting diodes, spin-valve transistors, new functionality of memory detectors, logic devices and light-emitting sources are being investigated [2]. It is interesting to note that ferromagnetic semiconductors with Curie temperature around 300 K may be obtained by doping conventional semiconductors with transition metal ions. The ferromagnetic interaction between the magnetic ions mediated by charge carriers enables one to manipulate both the charge and spin degrees of freedom of electrons. Most of the efforts have been initially focused on Mn-substituted III–V compounds such as $Ga_{1-x}Mn_xAs$, which are normally p-type and exhibit ferromagnetism around 110 K [3]. This has hindered their applications because room temperature ferromagnetism is desired for new generation spintronic devices. In view of this, there have been many reports [4–10] to produce RTFM materials, particularly wide band gap II–VI semiconductors such as ZnO, TiO_2, SnO_2 ZnS, ZnSe and ZnTe doped with a few at% of 3d transition-metal ions like Mn, Fe, Co, Cr, Ni, Cu, etc. Some progress has been made to realize spintronic devices in practice

*Corresponding author. Tel.: +82 10 31 330 4762.
E-mail address: dranreddysvu@gmail.com (D. A. Reddy).

0272-8842/$ - see front matter © 2013 Elsevier Ltd and Techna Group S.r.l. All rights reserved.
http://dx.doi.org/10.1016/j.ceramint.2013.07.006

using the room temperature ferromagnetic DMS materials [11]. However, new generation spintronic device fabrication calls for materials exhibiting enhanced magnetic and optical properties. In this pursuit co-doping of two different types of ions into a host semiconducting nanocrystals to tune their luminescent and magnetic properties has been tried [12–15]. Till now the work has been almost entirely concerned with n-type materials, which raises important and interesting scientific issues concerning the carrier-mediated magnetism. However, n-type (donars) and p-type (acceptors) dopants incorporated into nanocrystals could presumably provide extra charge carriers, electrons or holes to the semiconductor lattice, which could be extremely important for electrical transport in nano-crystalline devices. In view of these a few studies [16–18] have been undertaken on co-doping of p-type and n-type materials and some progress has been achieved in this direction. Among all the co-doping systems, particularly Al co-doping is very interesting because many authors reported varying incongruous results for seemingly identical materials. Liu et al. [19] found high-temperature ferromagnetism in (Co, Al) co-doped ZnO nano-powders. Pei et al. [20] reported absence of RTFM in Al co-doped ZnO:Co nanoparticles. Ning et al. [21] reported enhanced ferromagnetism in Al co-doping and Wei et al. [22] reported reduced ferromagnetisam with Al co-doping. However surprisingly as per our knowledge, there are no experimental reports on magnetic studies on Al co-doped ZnS nanoparticles, although the above mentioned experimental results indicate the possibility of room temperature ferromagnetism in ZnS, which is similar to ZnO. We have reported earlier [23] dopant induced room temperature ferromagnetism in Cr doped ZnS nanoparticles. It is interesting to note that ferromagnetism was suppressed appreciably at higher doping concentration of Cr (3 at%) compared to 0.5 at%. Also, the present authors investigated ZnS:(Cr, Cu) [12] and ZnS:(Cr, Mn) [13] nano-systems and observed enhanced RTFM in Cu co-doped samples whereas in Mn co-doped samples suppression of RTFM was noticed. Hence in the present study, out of curiosity we have chosen to investigate the effect of Al co-doping on the weakest ferromagnetic samples of ZnS:Cr (3 at% Cr). The authors have undertaken the synthesis of (Cr, Al) co-doped ZnS nanoparticles using the simple and inexpensive technique namely the chemical co-precipitation method. The nanoparticles have been subjected to structural, optical and magnetic characterizations and the observations are reported in this paper.

2. Experimental

For the synthesis of nanostructured ZnS:(Cr, Al) particles we followed a similar procedure reported earlier [12,13,23]. In brief all the chemicals used in the present work were of analytical grade and were used without further purification. Ultra-pure de-ionized water was used in all synthesis steps. In this study $Zn_{0.97-x}Al_xCr_{0.03}S$ (x=0.00, 0.02, 0.04, 0.06, 0.08, 0.10, and 0.12) nanocrystals were synthesized using $Zn(CH_3COO)_2$, Na_2S as the precursors and $CrCl_3 \cdot 6H_2O$ and $Al_2(SO_4)_3$ as the source of dopant material. ZnS:(Cr, Al) nanoparticles were synthesized using EDTA as the capping agent. The source materials were weighed according to the stoichiometry as per the target compositions and were dissolved in distilled water to make a 0.2 M solution. Sodium sulfide and Cr and Al solutions were added simultaneously dropwise to the zinc acetate solution under continuous stirring for 8 h at room temperature till a fine precipitate was formed. The precipitate was filtered out separately and washed with de-ionized water and methanol to remove unnecessary impurities formed during the preparation process. The obtained product was placed in oven for 6 h at 60 °C. Chemical analysis and morphology was carried out using Scanning Electron Microscopy (SEM) with EDAX attachment (CARL-ZEISS EVO MA 15). The X-ray diffraction (XRD) patterns were recorded to study the phase and structure of the nanoparticles using Seifert 3003 TT X-Ray Diffractometer. Transmission electron microscopy (TEM) were recorded in (JEOL-TEM 2010) with an accelerating voltage of 200 kV. Diffuse reflectance measurements (DRS) on dry powders were performed using a JASCO-V-670 double-beam spectrophotometer. Photoluminescence studies were carried out using a JOBIN YVON Fluorolog-3 Spectophotometer with 450 W of Xenon arc lamp as an excitation source. FTIR spectra were recorded using Thermo Nicolet FTIR-200 of thermo Electron Corporation. Electron paramagnetic resonance spectral (EPR) studies were done at room temperature using a JEOL-FE1X EPR spectrometer. To know the magnetic state of the samples prepared, room temperature magnetization was studied as a function of applied magnetic field in the range of −15,000 to +15,000 G using a Lakeshore Vibrating sample magnetometer, VSM-7410.

3. Results and discussion

3.1. Elemental analysis

The elemental analysis of ZnS:(Cr, Al) nanoparticles was done by EDS. Fig. 1(a) and (b) shows typical EDS spectra of ZnS:Cr and ZnS:(Cr, Al) nanoparticles, respectively. The spectra reveal that only the expected elements, Zn, S and Cr, are present in ZnS:Cr and that in addition Al element exists in ZnS:(Cr, Al) samples. No traces of other elements were noticed in the spectra indicating the purity of the samples. Quantitative analysis of the atomic concentration (at%) is listed in Table 1. The estimated Cr and Al concentrations are near to stoichiometry indicating that most of the Cr and Al ions exist in ZnS:(Cr, Al) nanocrystallites rather than in the form of hydroxides. However, the estimated dopant ion concentrations are slightly less than the nominal values indicating that some of the Cr and Al ions still remained in the parent solution and had not been incorporated into the crystals. The relative error is less than $\pm 0.5\%$.

3.2. Morphological studies

The morphological and elemental mapping features of the $Zn_{0.91}Al_{0.06}Cr_{0.03}S$ nanoparticles were examined using SEM analysis. Typical SEM images of ZnS:(Cr, Al) nanoparticles with elemental mapping are shown in Fig. 2(a–e). It can be seen from the SEM images that the particles coalesce to form

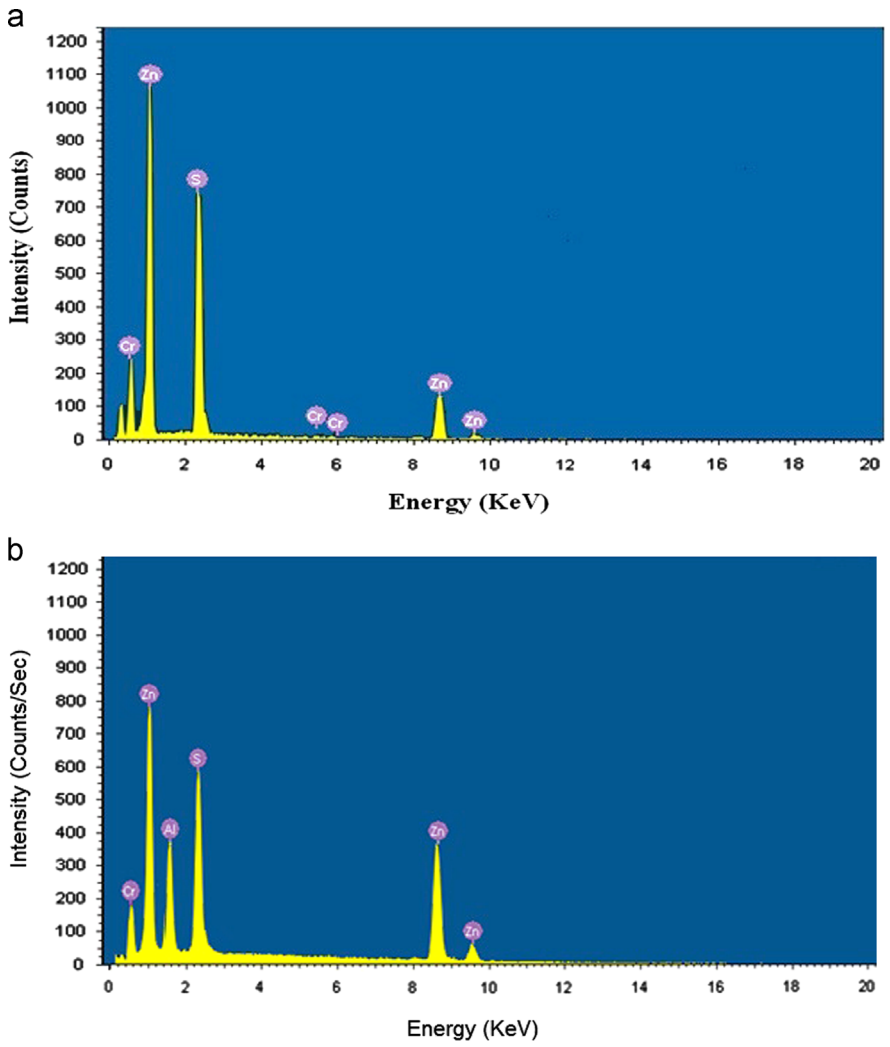

Fig. 1. EDS spectra of (a) ZnS:Cr and (b) $Zn_{0.93}Al_{0.04}Cr_{0.03}S$ nanoparticles.

Table 1
Estimated composition, crystallite size, lattice parameters and band gap of $Zn_{0.97-x}Al_xCr_{0.03}S$ nanoparticles.

Composition (x)	Estimated composition from EDS				Crystallite size (D) (nm)	Lattice parameter (a) (Å)	Band gap (eV)
	Zn	S	Cr	Al			
0.00	47.41	49.62	2.97	0.0	6.19	5.1930	4.05
0.02	45.71	49.48	2.98	1.83	6.26	5.1932	4.00
0.04	43.76	49.12	2.82	3.89	6.88	5.1934	3.97
0.06	42.06	48.98	2.98	5.98	7.12	5.1935	3.93
0.08	40.46	48.86	2.86	7.82	7.34	5.1937	3.89
0.10	38.07	49.56	2.74	9.63	7.85	5.1938	3.85

agglomerations with size ranging from 100 to 200 nm. The agglomerations might have originated from the large surface area and high surface energy of ZnS nanoparticles. From the elemental mapping, we observed that all the elements are consistently distributed over the field of view of the image. The elemental analysis of the images further showed that the nanoparticles were slightly rich in Zn and S compare to Al, and Cr. Further it clearly indicates quite a uniform distribution of elements in the synthesized products and demonstrates that the ZnS nanocrystals are homogenously doped with Al and Cr.

3.3. Structural analysis

X-ray diffractograms were used to investigate the effect of Al co-doping on the structure and the phase purity of the nanoparticles. Fig. 3 shows the XRD patterns of $Zn_{0.97-x}Cr_{0.03}Al_xS$

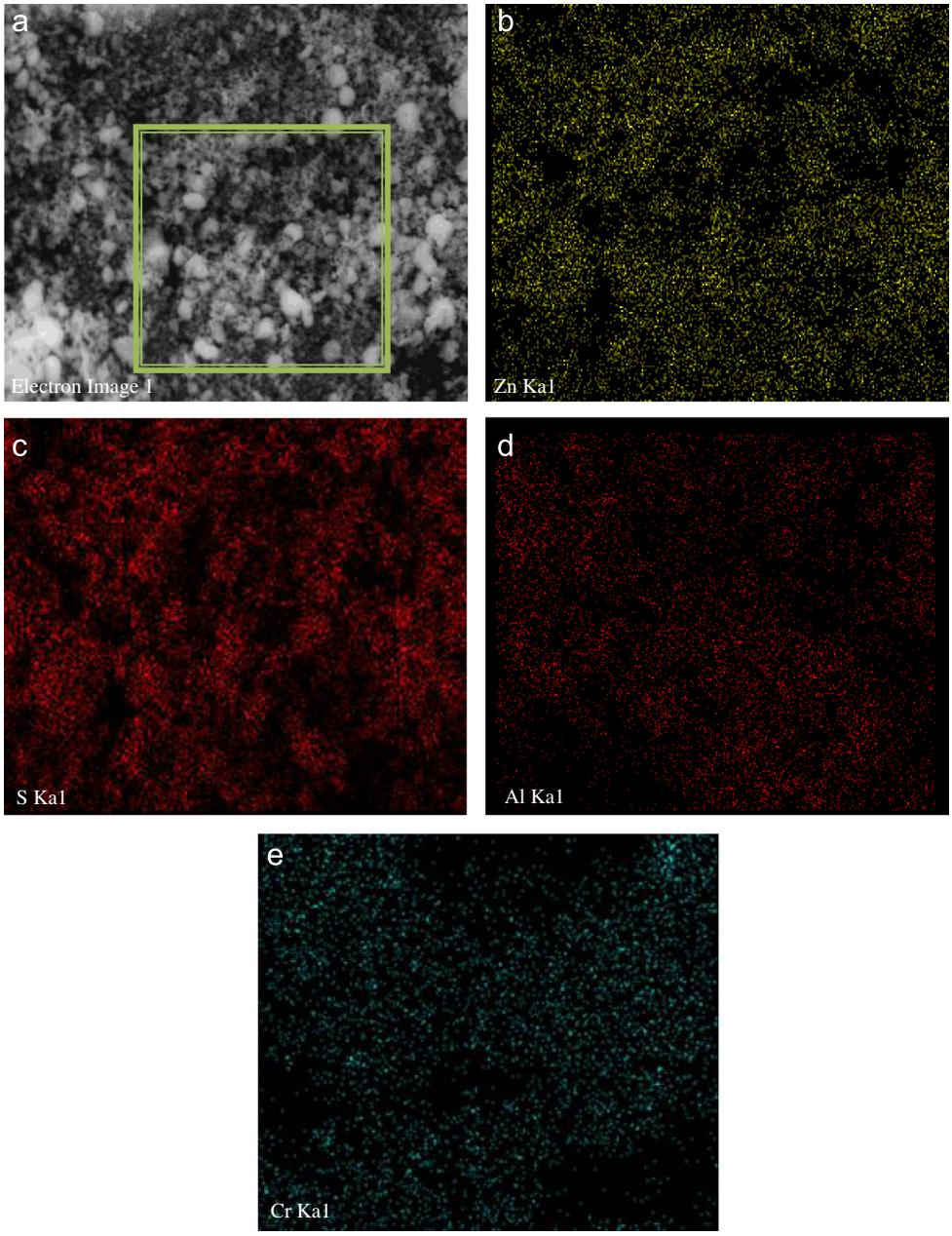

Fig. 2. (a) Electron micrograph and elemental mapping of 6 at% Al-doped ZnS:Cr sample showing the presence of (b) Zn (c) S (d) Al and (e) Cr ions, respectively.

(x=0.00, 0.02, 0.04, 0.06, 0.08, 0.10, and 0.12). For x=0.00–0.10 all peak positions of the present samples match well with the standard JCPDS no (80-0020) for cubic ZnS. No traces of chromium metal, aluminum metal or any other impurities are detected indicating that both Cr and Al have entered the ZnS host lattice as substituents. However, in samples of $Zn_{0.85}Al_{0.12}Cr_{0.03}S$ a secondary phase of Al_2S_3 is noticed. Therefore, it may be concluded that the doping limit for Al in ZnS:Cr is 10 at%. The average nanocrystallite size (D), was estimated from the full width at half maximum (FWHM) of the most prominent XRD (111) peak using Debye–Scherrer's formula, $D=0.89\lambda/\beta \cos\theta$, where λ is the wavelength of Cu-Kα irradiation and "θ" is diffraction angle for the (111) planes of cubic ZnS, and is presented in Table 1. The table indicates a steady increase of "D" with increasing Al concentration. Earlier workers also reported similar increase in crystallite size in co-doped ZnS:(Cu, Cd) [24], ZnS:(Cu, In) [25], ZnS:(Cr, Cu) [12] and ZnS:(Cu, Co) [26]. The XRD peaks (Fig. 3) show a slight shift towards lower 2θ values, implying an increase in lattice parameters on co-doping. The lattice parameter (a) of cubic zincblende is calculated from the formula: $1/d^2=1/a^2(h^2+k^2+l^2)$ where d_{hkl} is the inter planar separation corresponding to Miller indices (hkl) and is given in Table 1. From the table it is obvious that as the Al concentration increases, the lattice parameter slightly increases. This is expected because ions of smaller ionic radii, Al^{3+} (0.51 Å) and Cr^{3+} (0.63 Å), are replacing Zn^{2+} (0.74 Å). The increase in crystallite size as a result of Cr and Al substitution at Zn sites could be correlated with the increase in lattice parameters; it is a clear evidence that Cr and Al ions are substituting Zn in ZnS matrix. No data on lattice parameter of Al co-doped ZnS nanoparticles is

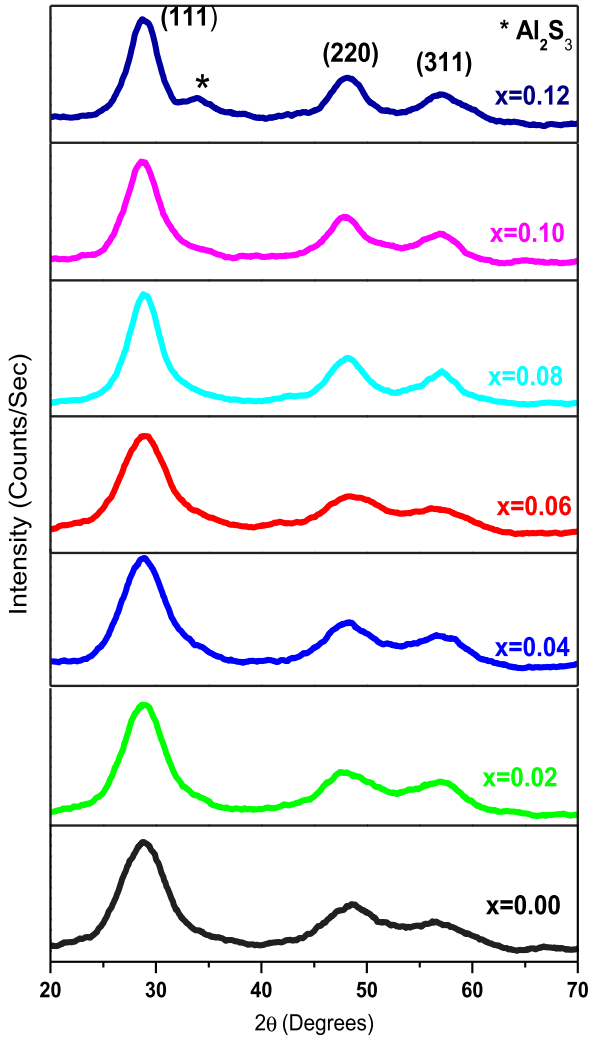

Fig. 3. X-ray diffraction patterns of $Zn_{0.97-x}Al_xCr_{0.03}S$ nanoparticles.

available for comparison. However, in a similar system of ZnO, Pei et al. [20] also reported such increase in lattice parameter in (Co, Al) co-doped ZnO nanoparticles.

3.4. TEM analysis

The TEM measurements were also performed to confirm the nanocrystalline nature and to study the morphology of the particles. Typical TEM micrograph of ZnS:(Cr, Al) ($x=0.06$) is shown in Fig. 4(a). In all the samples, the grains are found to be well isolated and nearly spherical in shape. The grain size values estimated from TEM images are in agreement with those obtained from XRD patterns. The SAED patterns for $x=0.06$ are shown in Fig. 4(b). From the SAED rings it is noticed that ZnS:(Cr, Al) samples of all compositions have zincblende structure with diffraction planes (111), (220) and (311) (JCPDS card no. 80-0020). Further, the presence of any secondary phase corresponding to Cr clusters or aluminum clusters was not detected in the XRD and TEM patterns. This indicates that Cr and Al have entered the ZnS host lattice as substituents and also that there are no other impurities present in the samples.

3.5. DRS studies

In order to study the effect of Al co-doping on band gap, UV–vis spectroscopic measurements were carried out at room temperature in the wavelength range 250–800 nm. The UV–vis diffuse reflectance spectra of $Zn_{0.97-x}Al_xCr_{0.03}S$ nanoparticles are shown in Fig. 5. It is obvious from the spectra that as the Al doping concentration increases the absorption edge shifts to higher wavelengths indicating a decrease in band gap with increasing dopant concentration. The shift in the absorption edge may be due to the increase of crystallite size with increasing Al concentration. The energy gap of the samples was determined by using the Kubelka–Munk equation,

$$\mathrm{Log}\left[\frac{(1-r)^2}{2r}\right] = \mathrm{Log}k - \mathrm{Log}s$$

where $r=R(\text{sample})/R(\text{standard})$

Here, the standard used is $BaSO_4$. R (standard) is taken as unity. R (sample) is the diffuse reflectance of the sample ($R=I\text{sam}/I\text{ref}$).

$$\frac{(1-R)^2}{2R} = \frac{k}{s} = F(R)$$

where "s" represents the portion of light scattered per unit vertical length, "k" represents the portion of light absorbed per unit vertical length, R is the reflectance relative to a standard and $F(R)$ is the remission function of the electrode. The Kubelka–Munk model assumes that the material is infinitely thick, and the thickness and surrounding apparatus have no influence on the reflectance [27]. The band gap of single phase semiconducting material and the absorption threshold of composite electrodes can be evaluated by plotting $[F(R)h\nu]^2$ vs. $h\nu$ for direct band gap materials. The band gap energies of $Zn_{097-x}Al_xCr_{0.03}S$ samples were estimated from the variation of the Kubelka–Munk fuction $[F(R)h\nu]^2$ with photon energy ($h\nu$), which is represented in Fig. 6. The estimated band gap energies are listed in Table 1. The table shows that as the Al concentration increases the band gap decreases from 4.05 to 3.85 eV, indicating that Cr and Al ions replace Zn^{2+} ions in the ZnS lattice and the energy band gap decreases on co-doping. Earlier workers also reported similar decrease in band gap after co-doping with different transition ions in ZnS [12,24–26]. There are no reports on band-gap studies of (Cr, Al) co-doped ZnS nanoparticles for comparison.

3.6. FTIR studies

Fourier transform infrared spectra (FTIR) is a versatile technique and gives detailed information about the chemical bonding and the elemental constituents of a material. Fig. 7 shows FTIR spectra of $Zn_{0.97-x}Al_xCr_{0.03}S$ (x=0.00, 0.02, 0.04, 0.06, 0.08 and 0.10) nanoparticles. The broad absorption peak

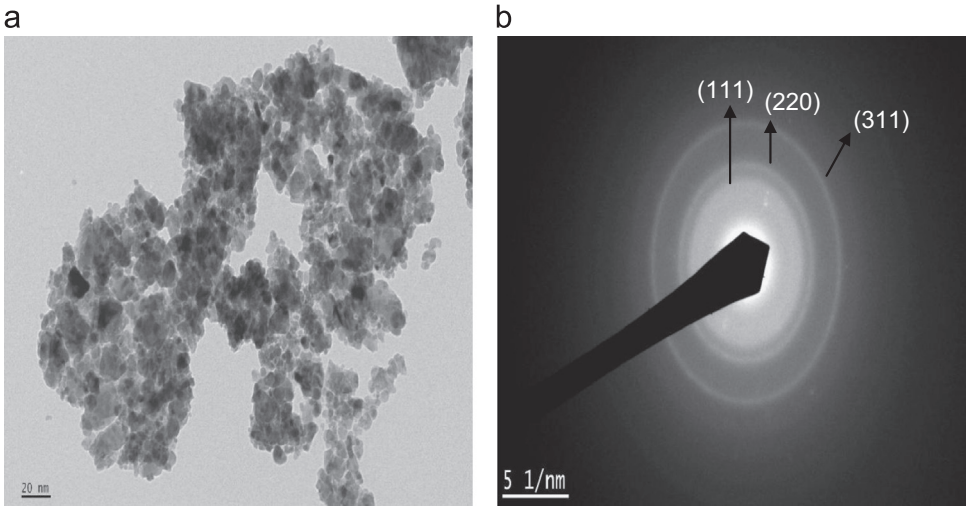

Fig. 4. (a) TEM and (b) SAED patterns of $Zn_{0.91}Al_{0.06}Cr_{0.03}S$ nanoparticles.

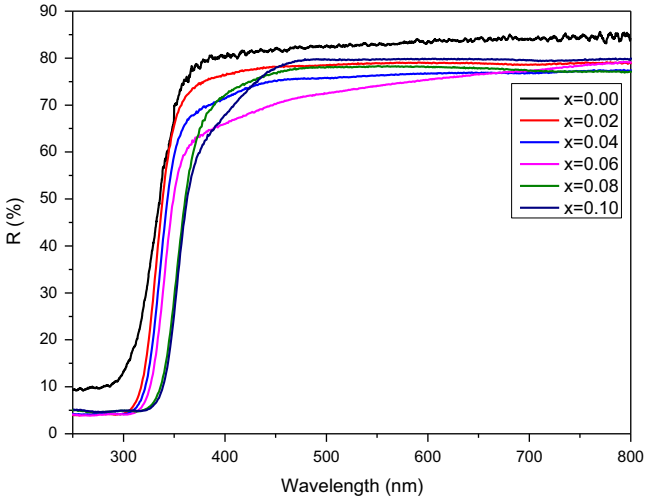

Fig. 5. DRS spectra of $Zn_{0.97-x}Al_xCr_{0.03}S$ nanoparticles.

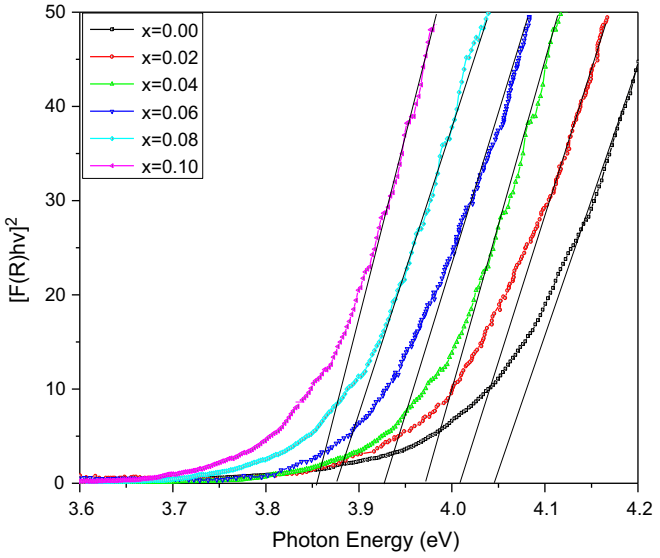

Fig. 6. Kubelka–Munk plots and band gap energy estimation for $Zn_{0.97-x}Al_xCr_{0.03}S$ nanoparticles.

around 3410 cm^{-1} is attributed to normal polymeric O–H stretching vibration of H_2O in ZnS:(Cr, Al) lattice because all FTIR spectra are recorded by mixing samples with KBr, which is hygroscopic. The spectral band located at 2352 cm^{-1} is related to N–H_3^+ stretching vibration of the amino acid. The most intense bands at 1580 cm^{-1} and 1410 $cm^{-1}$are the asymmetric and symmetric stretches of the coordinated carboxylate groups respectively [28]. Absence of spectral band around 2100 cm^{-1} indicates that in ZnS:(Cr, Al) matrices, EDTA does not form any betaine structure. However, the bands at 1580 cm^{-1} and 1400 cm^{-1} indicate that the EDTA carboxylate ions are active in the ZnS:(Cr, Al) matrices [12,13]. The spectral band at 1103 cm^{-1} is attributed to C–O stretching of carboxylic acid related to ZnS:(Cr, Al)–EDTA [23]. The spectral bands at 670 and 470 cm^{-1} are assigned to the Zn–S stretching vibrations [29]. These IR spectra strongly support that the surface capping of the ZnS nanoparticles is by direct bonding of the EDTA, to the ZnS site at the surface and does not interact chemically. This implies that EDTA simply co-exists with the surface of the nanoparticles and acts as surfactant and prevents the agglomeration of the nanoparticles.

3.7. Photoluminescence studies

The excitation spectra of ZnS:Cr and ZnS:(Cr, Al) nanoparticles in the wavelength range of 250–400 nm shown in Fig. 8 indicate excitation maximum at 334 nm. The excitation spectrum of the ZnS:Cr nanoparticles is considerably broadened compared to those of ZnS:(Cr, Al) nanoparticles. This broadening is mainly due to the strongly disordered surface which generates an individual random potential in each nanoparticle. This random potential induces enhanced fluctuations in the energy levels between different nanoparticles. The fluctuations of the levels increase with decreasing size of the particles, i.e., the excitation spectra broaden with decreasing

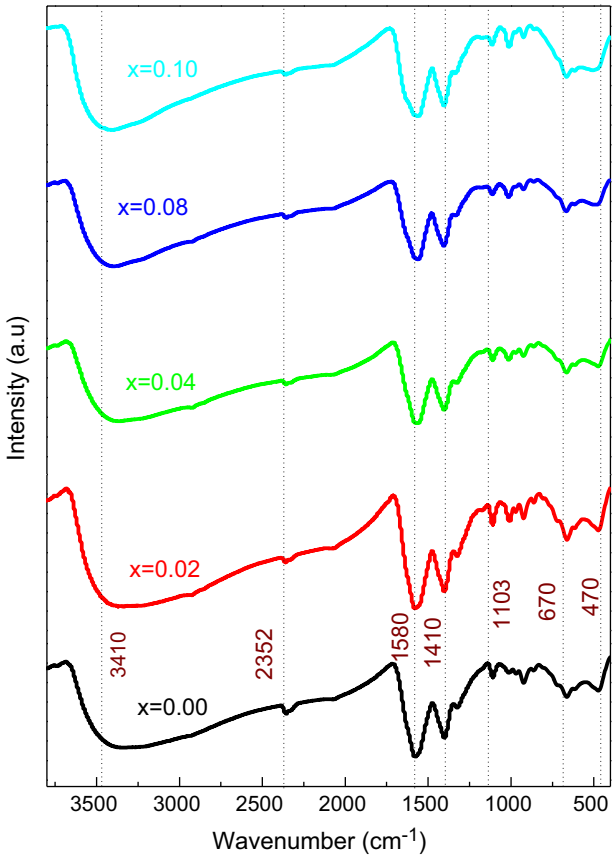

Fig. 7. FTIR spectra of $Zn_{0.97-x}Al_xCr_{0.03}S$ nanoparticles.

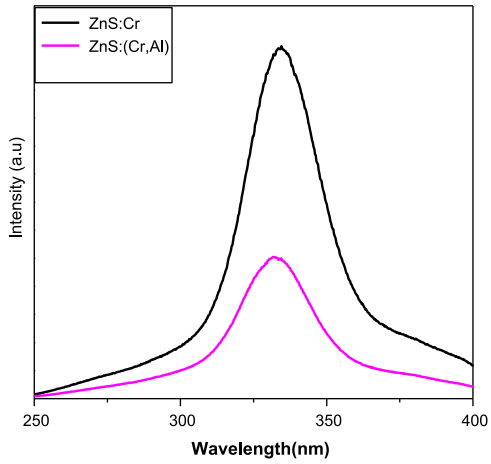

Fig. 8. Excitation spectrum of ZnS:Cr and ZnS:(Cr, Al) nanoparticles.

size. This effect is produced by the higher probability of smaller particles existing on the disordered surface [30].

To study the influence of Al co-doping in ZnS:Cr nanoparticles on emissions and defect formation, PL spectra of $Zn_{0.97-x}Al_xCr_{0.03}S$ nanoparticles were recorded at room temperature with an excitation wavelength of 334 nm and are shown in Fig. 9. It is observed that the PL spectra of ZnS:Cr nanoparticles consist of an emission band peaking at 445 nm and a very broad deep level emission band in the range of 400–630 nm. The emission appearing in the blue region of the visible spectrum can be ascribed to a self-activated center presumably formed between a Zn vacancy and a shallow donor associated with a sulfur vacancy [31,12,13]. Sulfur vacancies at the surface are expected to give rise to Zn dangling bonds that form shallow donor levels. Thus, the recombination is mainly between these shallow donor levels and the valence band arising from a very fast energy transfer from the electron hole pair excited across the band gap of the nanocrystals. In ZnS:(Cr, Al) samples an increase in emission intensity with Al content is noticed, with the PL peak slightly shifted to 470 nm. The PL at 470 nm may be due to the self-activated luminescence, with the incorporation of Al into ZnS structure that resulted from the donor–acceptor pair (DAP) transition. Nagamani et al. [32] also reported similar type of emission in Al doped ZnS thin films formed by the solution growth method. This provides an obvious evidence for the entry of aluminum in host lattice. Although the emission spectra of Al co-doped samples appear similar, an appreciable luminescence enhancement was observed in Al co-doped samples compared to the ZnS:Cr samples. The enhanced emission upon Al doping can be attributed to several factors such as (i) it is obvious that Al^{3+} is acting as a sensitizing agent enhancing the radiative recombination processes. Thus, the photoluminescence efficiencies of ZnS:(Cr, Al) samples are higher than those of ZnS:Cr samples. (ii) Increase of electron population in conduction band with doping of donor impurities. (iii) Higher rate of donor bound excitonic recombination (iv) and also sulfur vacancies are dominant in our samples with more sulfur vacancies being produced by the introduction of Al. All these factors might have enhanced the probability of enhanced of luminescence. The intensity of this visible emission decreases for samples with 6–10 at% Al doping. Such anomalous intensity variation in Al co-doped ZnS:Cr nanoparticles can be understood considering the possibility of Al entering at interstitial sites. While for low doping concentrations 0–4 at% most of the Al ions might have been incorporated into the ZnS

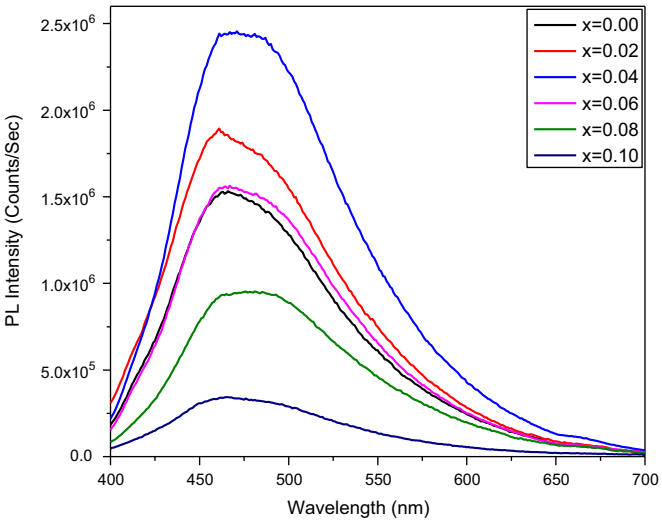

Fig. 9. PL spectra of $Zn_{0.97-x}Al_xCr_{0.03}S$ nanoparticles.

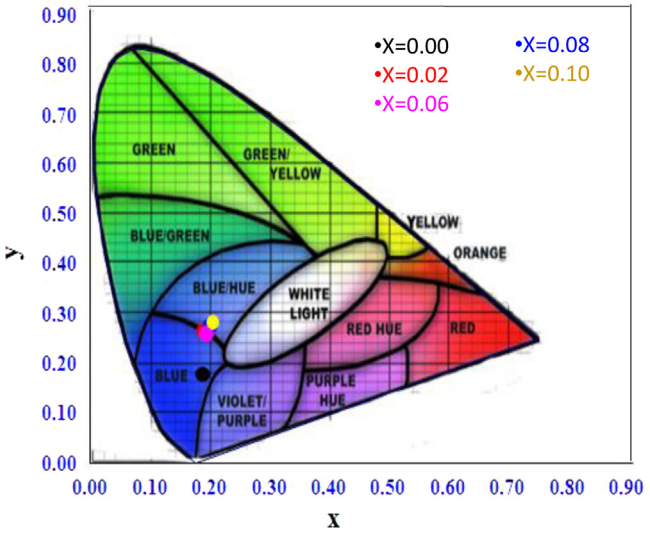

Fig. 10. CIE chromaticity diagram for $Zn_{0.97-x}Al_xCr_{0.03}S$ nanoparticles.

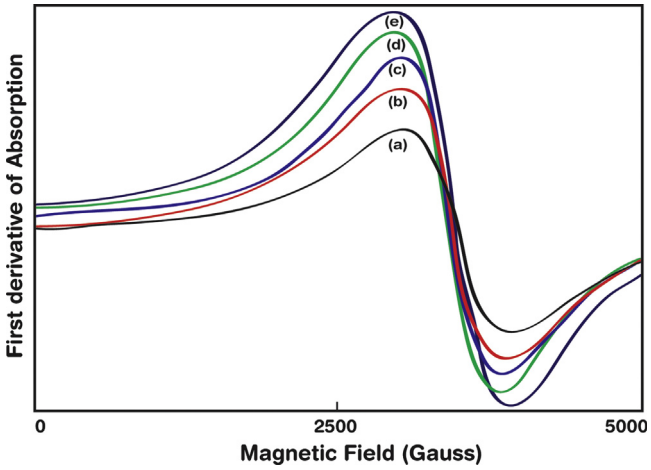

Fig. 11. EPR spectra of $Zn_{0.97-x}Al_xCr_{0.03}S$ (a) $x=0.00$, (b) $x=0.02$, (c) $x=0.04$, (d) $x=0.08$ and (e) $x=0.10$ nanoparticles.

lattice through substitution, for higher concentrations, the excess amount of Al ions might have been incorporated in to the nanoparticles interstitially, the interstitially doped Al atoms creating larger amount of lattice defects. Hence at higher concentrations of Al doping the photoluminescence intensity decreases. The presence of metallic Al peaks in the XRD patterns of the Al doped samples at 12 at% supports our argument.

The Commission International de l′Eclairage (CIE) color coordinates measured from the photoluminescent emission of Cr-doped ZnS nanoparticles and Al co-doped ZnS:Cr by varying the Al dopant concentrations are shown in Fig. 10. Compared to the Cr-doped ZnS nanoparticles in Al co-doped samples the CIE position shifted to strong blue region.

3.8. EPR studies

Electron Paramagnetic Resonance (EPR) is a purely quantum mechanical effect. It gives information regarding the oxidation state and site occupancy of the transition metal ion in the host lattice and the interplay between the carrier concentration and magnetic exchange coupling at microscopic level. EPR spectra of (Cr, Al) co-doped ZnS nano-powders were recorded at room temperature using a JEOL-FE1X EPR spectrometer operating in the X-band frequency (9.205 GHz) with a field modulation frequency of 200 KHz. The magnetic field applied was in the range of 0–5000 G and the microwave power used was 10 mW. Fig. 11 shows the EPR spectra of $Zn_{0.97-x}Al_xCr_{0.03}S$ ($x=0.00$, 0.02, 0.04, 0.08, and 0.10) nanopowders recorded at room temperature with magnetic fields applied in-plane (||) and perpendicular ($\perp$) to the sample. Generally EPR spectrum of Cr^{3+} gives three lines, arising from the $3d^3$ electronic configuration of Cr ion with spin $I=3/2$. Similarly Cr^{2+} gives four lines due to $3d^4$ electronic configuration with spin $I=1/2$. Al^{3+} ions give two lines, arising from the $3d^4$ electronic configuration with spin $I=1/2$, but in our studies we obtained single broad EPR signal which is attributed to the exchange interaction between Cr–Cr, Al–Al ions. Further, a gradual increase in the intensity of the signal is noticed with increasing Al ion concentration indicating a gradual weakening of ferromagnetic ordering because of exchange interaction. The g-factor was determined from the equation of resonance $g=h\nu/\beta H$, where "g"$=g$-factor, $h=$Planck′s constant$=6.625\times10^{-34}$ m^2 kg/s, $\beta=$Bohr magneton 9.274×10^{-24} J T^{-1}, $\nu=$frequency, $H=$magnetic field in Tesla. The value of "g" obtained is in the range of 1.989–2.001. As the Al concentration increases the g-value increases as shown in Table 2. Hence, we assume that the resonance signal in the EPR spectrum is related to some of the Al and Cr ions in the paramagnetic state. The peak to-peak linewidth (ΔH) values of the hyperfine lines obtained from the EPR signals are found to increase with increase in Al concentration (Table 2). Generally the change in linewidth mainly depends on the variation of temperature and concentration of the dopants. In the present case all EPR studies are carried out at room temperature only. Hence the increase in ΔH is attributed to increased dipole–dipole interactions between Cr^{3+} and Al^{3+} ions and also due to inhomogenities in the internal field due to random distribution of Cr^{3+} and Al^{3+} ions.

The values of number of spins (N_s) participating in the resonance are calculated using the formula: $N_s=0.285I(\Delta H)^2$ where "I" is the peak-to-peak height and "ΔH" is the linewidth (in G) and are given in Table 2. The increase in broadening and intensity of the EPR signal with increasing Al concentration clearly indicates that there is an increase in the number of spins with increasing Al dopant content.

3.9. Magnetization studies

To know the magnetic state of the $Zn_{0.97-x}Al_xCr_{0.03}S$ ($x=0.00$, 0.02, 0.04, 0.06, 0.08, and 0.10) samples, room temperature magnetization is studied as a function of applied magnetic field in the range of −15,000 to +15,000 G using VSM and are shown in Fig. 12. From the figure it is clear that Cr doped ZnS nanoparticles exhibit room temperature ferromagnetism. The present authors explained the origin of

Table 2
Lande "g" factor, line width (ΔH) and Number of spins (N_s) of $Zn_{0.97-x}Al_xCr_{0.03}S$ nanoparticles.

Composition (x)	Lande "g" factor	Line width (ΔH) (Gauss)	Number of spins (N_s) (cm^{-1})
0.00	1.989	367	7.48×10^6
0.02	1.991	372	7.56×10^6
0.04	1.993	378	7.62×10^6
0.06	1.995	381	8.02×10^6
0.08	1.998	383	8.32×10^6
0.10	2.001	384	8.51×10^6

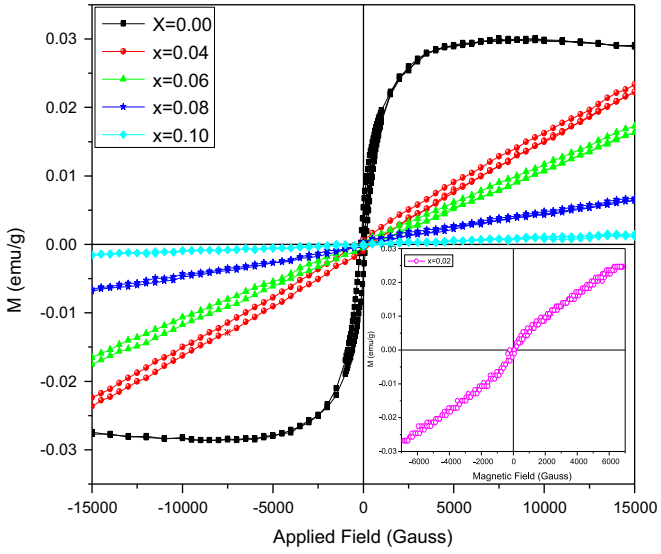

Fig. 12. Room temperature M–H loop for $Zn_{0.97-x}Al_xCr_{0.03}S$ nanoparticles.

ferromagnetism in Cr doped ZnS nanoparticles earlier [23]. In brief the observed ferromagnetism in Cr doped ZnS is due to the substitution of Cr for Zn which provides the necessary unpaired spins for ferromagnetism rather than the Cr clusters. Thus, the observed ferromagnetism in the Cr doped ZnS samples was attributed to the exchange interaction between localized "d" spins on the Cr ions and the free delocalized carriers. The values of coercive field (H_c), magnetization (M_s) and retentivity (M_r) of the Cr doped ZnS nanoparticles are 152.3 G, 27.9E−3 and 3.39E−3 respectively. A small amount of Al co-doping brought drastic changes in the magnetic properties. In samples with $x=0.02$ exhibit coexistence of paramagnetism as well as antiferromagnetism is observed as shown by the inset in Fig. 12. The change of magnetic behavior from ferromagnetic state to mixture of antiferromagnetic and paramagnetic states may be due to the interactions between the Cr–Cr ions, Al–Al ions and Cr–Al ions in co-doped samples. It may lead to lattice distortions and neighboring defects giving rise to changes in the magnetic nature. Pei et al. [20] also observed similar mixed state in ZnO:(Co, Al) co-doped samples. There are no reports of magnetic studies on (Cr, Al) co-doped ZnS nanoparticles for comparison. On increasing the Al concentration from $x=0.04$–0.10 the samples exhibited nearly zero coercivity and no remanent magnetization, which is typical of paramagnetism. The absence of room temperature ferromagnetism in Al co-doped ZnS:Cr nanoparticles may be due to the formation of very tiny nanometer sized Al clusters or other secondary phases that remain paramagnetic at room temperature. There are no earlier reports available for comparison. However, in a similar system of ZnO:(Co, Al), Alaria et al. [33] reported absence of room temperature ferromagnetism in Al co-doped ZnO:Co nanocrystals. More detailed investigations like low temperature magnetic studies are needed to understand the mechanism of magnetism in this material. Such investigations are under progress in our laboratory.

4. Conclusions

$Zn_{0.97-x}Al_xCr_{0.03}S$ nanoparticles were synthesized by the chemical co-precipitation method using EDTA as the capping agent. EDS, XRD and FTIR studies reveal that Cr and Al are incorporated into the ZnS host lattice without altering the crystal structure. With Al co-doping, the band gap varied in the range of 4.05–3.85 eV. Enhanced photo luminescence with increase in Al co-doping was observed up to 4 at% and beyond 4 at% luminescence quenching was observed. FTIR spectra indicate that the EDTA simply co-exists on the surface of nanostructures and acts as a capping agent and inhibits the agglomeration of the nanoparticles. As the Al co-doping concentration increases the EPR signal intensity, linewidth, Lande "g" value, the number of spins increases providing evidence for the presence of paramagnetic ions in the prepared samples. The absence of room temperature ferromagnetism observed in Al co-doped samples indicates that Al co-doping suppresses the RTFM of ZnS:Cr nanoparticles

Acknowledgment

This work was supported by Hankuk University of Foreign Studies Research Fund of 2013. The authors are thankful to Prof. J.L. Rao, S.V. University, Tirupati, India for his help in recording ESR spectra.

References

[1] J.K. Furdyna, Diluted magnetic semiconductors, Journal of Applied Physics 64 (1988) R29–R64.
[2] David D. Awschalom, Michael E. Flatte, Challenges for semiconductor spintronics, Nature Physics 3 (2007) 153–159.

[3] Takashi Hayashi, Yoshiaki Hashimoto, Shingo Katsumoto, Yasuhiro Iye, Effect of low-temperature annealing on transport and magnetism of diluted magnetic semiconductor (Ga,Mn)As, Applied Physics Letters 78 (2001) 1691–1693.
[4] Baiqi Wang, Javed Iqbal, Xudong Shan, Guowei Huang, Honggang Fu, Ronghai Yu, Dapeng Yu, Effects of Cr-doping on the photoluminescence and ferromagnetism at room temperature in ZnO nanomaterials prepared by soft chemistry route, Materials Chemistry and Physics 113 (2009) 103–106.
[5] Gunjan Srinet, Prateek Varshney, Ravindra Kumar, Vivek Sajal, P. K. Kulriya, M. Knobel, S.K. Sharma, Structural, optical and magnetic properties of $Zn_{1-x}Co_xO$ prepared by the sol–gel route, Ceramics International 39 (2013) 6077–6085.
[6] Jasneet Kaur, Jyoti Shah, R.K. Kotnala, Kuldeep Chand Verma, Raman spectra, photoluminescence and ferromagnetism of pure, Co and Fe doped SnO_2 nanoparticles, Ceramics International 38 (2012) 5563–5570.
[7] Z.M. Tian, S.L. Yuan, J.H. He, P. Li, S.Q. Zhang, C.H. Wang, Y. Q. Wang, S.Y. Yin, L. Liu, Structure and magnetic properties in Mn doped SnO_2 nanoparticles synthesized by chemical co-precipitation method, Journal of Alloys and Compounds 466 (2008) 26–30.
[8] Sandeep K.S. Patel, Sajith Kurian, Namdeo S. Gajbhiye, Room-temperature ferromagnetism of Fe-doped TiO_2 nanoparticles driven by oxygen vacancy, Materials Research Bulletin 48 (2013) 655–660.
[9] Sanjeev Kumar, C.L. Chen, C.L. Dong, Y.K. Ho, J.F. Lee, T.S. Chan, R. Thangavel, T.K. Chen, B.H. Mok, S.M. Rao, M.K. Wu, Room temperature ferromagnetism in Ni doped ZnS nanoparticles, Journal of Alloys and Compounds 554 (2013) 357–362.
[10] Pushpendra Kumar, Kedar Singh, Room temperature ferromagnetism in magic-sized Cr-doped CdS diluted magnetic semiconducting quantum dots, Journal of Nanoparticle Research 13 (2011) 1613–1620.
[11] S.D. Sarma, J. Fabian, X. Hu, I. Zutic, Spin electronics and spin computation, Solid State Communications 119 (2001) 207.
[12] D. Amaranatha Reddy, G. Murali, B. Poornaprakash, R.P. Vijayalakshmi, B. K. Reddy, Structural, optical and magnetic properties of $Zn_{0.97-x}Cu_xCr_{0.03}S$ nanoparticles, Applied Surface Science 258 (2012) 5206–5211.
[13] D. Amaranatha Reddy, S. Sambasivam, G. Murali, B. Poornaprakash, R.P. Vijayalakshmi, Y. Aparna, B.K. Reddy, J.L. Rao, Effect of Mn co-doping on the structural, optical and magnetic properties of ZnS:Cr nanoparticles, Journal of Alloys and Compounds 537 (2012) 208–215.
[14] Fengchun Hu, Qinghua Liu, Zhihu Sun, Tao Yao, Zhiyun Pan, Yuanyuan Li, Jingfu He, Bo He, Zhi Xie, Wensheng Yan, Shiqiang Wei, Cu and Co codoping effects on room-temperature ferromagnetism of (Co,Cu):ZnO dilute magnetic semiconductors, Journal of Applied Physics 109 (2011) 103705–103708.
[15] Xiaohu Huang, Guanghai Li, Lei Duan, Liang Li, Xincun Dou, Lide Zhang, Formation of ZnO nanosheets with room-temperature ferromagnetism by co-doping with Mn and Ni, Scripta Materialia 60 (2009) 984–987.
[16] Xinlong Tian, Zhanchang Pan, Huangchu Zhang, Hong Fan, Xiangfu Zeng, Chumin Xiao, Guanghui Hu, Zhigang Wei, Growth and characterization of the Al-doped and Al–Sn co-doped ZnO nanostructures, Ceramics International 39 (2013) 6497–6502.
[17] C.W. Zou, L.X. Shao, L.P. Guo, D.J. Fu, T.W. Kang, Ferromagnetism and ferroelectric properties of (Mn, Li) co-doped ZnO nanorods arrays deposited by electrodeposition, Journal of Crystal Growth 331 (2011) 44–48.
[18] Mingpeng Yu, Hong Qiu, Xiaobai Chen, Hui Li, Wei Gong, Al and Ni co-doped ZnO films with room temperature ferromagnetism, low resistivity and high transparence, Materials Chemistry and Physics 126 (2011) 797–803.
[19] X.C. Liu, E.W. Shi, Z.Z. Chen, H.W. Zhang, B. Xiao, L.X. Song, High-temperature ferromagnetism in (Co, Al)-codoped ZnO powders, Applied Physics Letters 88 (2006) 252503–252505.
[20] Guangqing Pei, Changtai Xia, Feng Wu, Jun Xu, Absence of room-temperature ferromagnetism in Al-codoped $Zn_{0.95}Co_{0.05}O$ nanoparticles, Journal of Alloys and Compounds 467 (2009) 539–542.
[21] Xingzhi Ning, XiaoFang Liu, Ronghai Yu, Ji Shi, Yoshio Nakamura, Materials Transactions 51 (2010) 557–560.
[22] Wei Yanyan, Hou Denglu, Zhao Ruibin, Zhou zhenzhen, Zhen Congmian, Tang Guide, Structural and magnetic properties of cobalt and aluminum co-doped ZnO powders, Advanced Materials Research 47–50 (2008) 600–603.
[23] D. Amaranatha Reddy, G. Murali, R.P. Vijayalakshmi, B.K. Reddy, Room-temperature ferromagnetism in EDTA capped Cr-doped ZnS nanoparticles, Applied Physics A 105 (2011) 119–124.
[24] P. Yang, M. Lu, D. Xu, D. Yuan, C. Song, Photoluminescence characteristics of ZnS nanocrystallites co-doped with Cu^{2+} and Cd^{2+}, Journal of Physics and Chemistry of Solids 64 (2003) 155–158.
[25] P. Yang, M.K. Lu, C.F. Song, D. Xu, D. Yuan, X.F. Cheng, G.J. Zhou, Luminescence of Cu^{2+} and In^{3+} co-activated ZnS nanoparticles, Optical Materials 20 (2002) 141–145.
[26] P. Yang, M. Lu, G. Zhou, D. Yuan, D. Xu, Photoluminescence characteristics of ZnS nanocrystallites co-doped with Co^{2+} and Cu^{2+}, Inorganic Chemistry Communications 4 (2001) 734–737.
[27] A. Escobedo Morales, E. Sanchez Mora, U. Pal, Use of diffuse reflectance spectroscopy for optical characterization of un-supported nanostructures, Revista Mexicana de Fisica 53 (2007) 18–22.
[28] Krishna Kanta Haldar, Amitava Patra, Fluorescence enhancement and quenching of Eu^{3+} ions by Au–ZnO core-shell and Au nanoparticles, Applied Physics Letters 95 (2009) 063103.
[29] Maged El-Kemary, Hany El-Shamy, Fluorescence modulation and photodegradation characteristics of safranin O dye in the presence of ZnS nanoparticles, Journal of Photochemistry and Photobiology 205 (2009) 151–155.
[30] D.U. Saenger, G. Jung, M. Mennig, Optical and structural properties of doped ZnS nanoparticles produced by the sol–gel method, Journal of Sol–Gel Science and Technology 13 (1998) 635–639.
[31] D.Amaranatha Reddy, G. Murali, R.P. Vijayalakshmi, B.K. Reddy, B. Sreedhar, Effect of Cr doping on the structural and optical properties of ZnS nanoparticles, Crystal Research and Technology 46 (2011) 731–736.
[32] K. Nagamani, N. Revathi, P. Prathap, Y. Lingappa, K.T. Ramakrishna Reddy, Al-doped ZnS layers synthesized by solution growth method, Current Applied Physics 12 (2012) 380–384.
[33] J. Alaria, H. Bieber, S. Colis, G. Schmerber, A. Dinia, Absence of ferromagnetism in Al-doped $Zn_{0.9}Co_{0.10}O$ diluted magnetic semiconductors, Applied Physics Letters 88 (2006) 112503–112505.